Study on surrounding rock disturbance effect of multi-middle section combined backfilling mining in inclined iron ore

Hexuan Zhu[1,2] · Lijun Han[1,2] · Qingbin Meng[2] · Xingquan Li[1,2] · Maolin Tian[1,2] · Lingdong Meng[1,2]

Abstract

As a high-efficiency and low-consumption mining mode, multi-middle section combined backfilling mining (MMSCBM) is becoming more and more widely used in metal mines. The geological mining conditions of Baixiangshan Iron Mine were taken as the simulation prototype. Similar model tests and numerical simulation experiments were used to study the surrounding rock disturbance, stope stability, surrounding rock stress, overburden settlement, and dynamic deformation of the ground surface during the MMSCBM process. The evolution process of the stope instability: the stable stage of the pillar, the large deformation stage of the pillar, the failure of some pillars, and the overall failure of the pillar. MMSCBM effectively buffered the excavation's disturbance to the surrounding rock, adjusted the stress release mode, and changed the stress concentration area. The dynamic deformation laws of the overburden and the surface were summarized. The method of field monitoring was verified by numerical simulation calculation to study the disturbance degree of MMSCBM to the roadway and evaluate the safety of the roadway. This research has important significance and value for the wider application of the mining model.

Keywords Metal mine · Multi-middle section combined backfilling mining · Similar model test · Instability evolution process

Introduction

The underground mining of metal mines occupies a considerable proportion in resource exploitation. After years of development, the empty field method, caving method, and backfilling method have become the three main methods of underground mining (Yu and Counter 1983; Kurakami et al. 2008; Xu et al. 2017; Emad 2017; Yi et al. 2017). The metallogenic deposits of metal deposits are different from those of coal mines. Because the veins generally extend widely, they are usually divided into a number of middle sections, which are mined in the middle section, and the middle section is used for mining and backfilling

✉ Lijun Han
  hanlj@cumt.edu.cn

1 School of Mechanics and Civil Engineering, China University of Mining and Technology, Xuzhou 221116, Jiangsu, China

2 State Key Laboratory for Geomechanics and Deep Underground Engineering, China University of Mining and Technology, Xuzhou 221116, Jiangsu, China

operations by mining units such as panels and access roads (Uskov et al. 2017; Xu et al. 2012).

Many scholars have conducted research on various aspects of metal mine segmentation. Some scholars have comprehensively optimized the boundary selection and scheduling of the section mining mining operations (Copland and Nehring 2016). Other scholars, through theoretical analysis, indoor similar simulation tests, etc., studied the effect of the mining height of the high-segment height sublevel caving method on the overlying strata movement and underground pressure characteristics (Yang et al. 2018). Some scholars have proposed a new method of downhole backfilling that is close to mining and descending, and established a mechanical model of the confined beam of the backfill in a single roadway, and calculated the optimal bearing layer thickness of the overlying backfill (Feng et al. 2017). Single mid-section mining is the usual mode of mine mining design. Single or multiple stopes are arranged in one middle section for mining, mining and backfilling operations. Only in the transition of the transition section, there will be short-term double-segment production. This single-stage production is simple, safe, and secure, but too low production capacity seriously restricts the economic development of the mine for some large mines (Zhang et al. 2018; Song et al. 2011). Therefore, in actual production, more

than one middle section is simultaneously produced, which is the mode of MMSCBM in the actual sense (Lan et al. 2015). As a practice-oriented mining mode, MMSCBM has not been clearly recognized and has not been well solved for its disadvantages such as difficulty in mining, severe disturbance, prominent ground pressure, and poor safety of stope. At the same time, the law of overburden migration and surface deformation of large-area continuous mining such as MMSCBM has always been paid attention to, but there are few systematic studies (Deng et al. 2018; Li et al. 2013).

MMSCBM is the first of the Jinchuan No. 2 mining areas to use the non-retained ore column for large-scale ore-backfilling in the complex engineering geological conditions (Emad et al. 2015; Lu and Gao 2003). This mining method is as follows: firstly, gradually upward mining in each middle section, and transition from one middle section to two middle sections, and then from two middle sections to multiple middle sections for simultaneous mining. Each middle section influences each other, and the influence effects overlap each other. The integrity of the overlying rock layer is gradually destroyed, and the rock mass will produce many secondary structural surfaces such as separation cracks, and the range of influence gradually increases from deep to shallow, until it extends to the surface. Therefore, it is necessary to study the surrounding rock disturbance law, overburden settlement, and surface dynamic deformation in the middle section of combined backfilling mining (Zhu et al. 2017; Li et al. 2014). In this paper, the model test and numerical calculation method are used to analyze the variation law of surrounding rock disturbance and stress field and displacement field in MMSCBM, and the overlying strata settlement and dynamic displacement deformation law are summarized. It has been demonstrated that MMSCBM reduces the degree of disturbance to surrounding rock caused by mining by adjusting the stress release mode and changing the stress concentration area. In addition, numerical simulation calculations are used to demonstrate on-site monitoring to evaluate the safety of roadways in the MMSCBM mining mode. The above research shows that MMSCBM has good practicability for large-scale mining of metal mines.

Similar model test study

Design of physical similarity model

The plane strain simulation test bench model is KD-01. The General Staff Engineering Research Institute and the China University of Mining and Technology jointly developed. The total weight of the equipment is 6590 kg, the maximum load concentration is 1.0 MPa, the piston area of a single cylinder is 12.56 cm^2, and the maximum stroke of the loading cylinder is 200 mm. The maximum loading oil pressure is 16

MPa, and the maximum model size is 2.5 m (length) × 1.5 m (height) × 0.3 m (width). The main body consists of a model frame, a console, an oil pump, side columns, and moving beams. The top is provided with a hydraulic loading device with a loading function in the direction to ensure a good plane strain condition. The test bench is suitable for the simulation test of the overlying strata activity law, the stability of the stope, the law of mine pressure, and the interaction mechanism between the filling body and the surrounding rock.

Determination of similar model parameters

According to the in situ stress, the physical and mechanical properties of the rock, and the geometric size of the similar simulation test bench, the similarity constant calculation method is used to determine the similarity ratio between the actual prototype object and the physical model. The maximum model size of the plane strain simulation test bench is 2.5 m (length) × 1.5 m (height) × 0.3 m (width). The test plan simulates the actual prototype size of 500 m (length) × 300 m (height) × 60 m (width). L stands for length, m, h are footnotes and represent models and actual objects, respectively, and C_L stands for geometric similarity ratio, then:

$$C_L = \frac{L_m}{L_h} = \frac{1}{200} \tag{1}$$

The volume-weight similarity ratio of the model is:

$$C_m = \frac{m_m}{m_h} = \frac{\rho_m L_m^3}{\rho_h L_h^3} = C_L^3 \frac{\rho_m}{\rho_h} = \frac{1}{1.5} \tag{2}$$

According to the similarity principle and dimensional analysis, the stress similarity ratio and time similarity ratio are obtained:

$$C_F = C_L \cdot C_m = \frac{1}{300} \tag{3}$$

$$C_T = \sqrt{C_L} = \frac{1}{14.08} \tag{4}$$

The compressive strength and volume-weight are used to accurately determine the ratio of similar materials in the rock formation and the amount of coal materials according to the stress similarity ratio of 1/300. Based on the on-site mining progress, mining and filling are carried out according to the time ratio parameter of 1/14.08.

Similar models and stratigraphic stratification

A total of 11 ore bodies have been identified in the deposit, of which the No. I ore body is the main ore body, and the ore body reserves account for 98.9% of the total reserves of the deposit. The main ore body is endowed with the inner zone of

the diorite and sand shale contact zone. The veins extend at a maximum of 1780 m, with an average of 1630 m. The tendency is a maximum extension of 1130 m with an average of 950 m and a total inclination of 13°. The left and right sides of the ore body undulate to the north, and the elevation is −200∼ −600 m. The overall thickness of the ore body is also large, from 2.22 to 121.72 m, generally 5 to 40 m, with an average of 34.41 m. The thickness of a few regional ore bodies is 60∼70 m continuously. The thickest part of the ore body is in the positive contact zone of the western CK101∼CK6 exploration line, and the rest is in the middle of the CK105∼CK110 exploration line. The shape of the thickest part of the ore body is mainly controlled by the anticline structure of the mining area. The overall lateral direction is flat and arched, and the stability is good. The surrounding rock of the top and bottom plates is mainly diorite and hornfels, followed by sand shale. The diorite rock has a large change in its strength within the influence of mining, and its local appearance is softened. The roof shale of the ore body is partially weak due to muddy action near the ore body. The hornfels is the direct top plate and the rock core is broken.

The similarity model experiment of this subject is based on the geological section of the Baixiangshan No. 1 iron mine exploration hole (as shown in Fig. 1) to establish a physical similarity model. The main research object is the positive contact between the CK101∼CK105 exploration holes in the western part of the exploration hole. The elevation is from −500 to −420 m and the lateral extension is 400 m. In order to facilitate the construction and experimental operability of the physical similar model, the ore body and rock formation are simplified as necessary, and the simplified model is shown in Fig. 2.

Two XY-5 engineering drilling rigs were put into use for the engineering geological survey of the main and auxiliary wells from March 19 to May 27, 2016. In this survey, a total of 1214.0 m of drilling footage were completed, and 60 groups of rock samples and 2 groups of water samples were collected. A series of tests were carried out, and all the work is detailed in Table 1.

The rock formations within the similar model were divided into four types according to the drilling data and rock test results, the geological age, sequence, genesis, mineral composition, and water richness of the rock formations. These four types of rock layers are quartz sandstone, angle shale, iron ore body, and diorite from top to bottom. Based on the actual rock formation conditions, the physical and mechanical parameters of the rock formation were reduced. Mica powder was arranged between the rock formations to play a layering role. Due to the low mechanical parameters of the rock mass of the mine and the relatively small stress, the mechanical parameters of the similar materials after conversion are very low. Therefore, the compressive strength and volume-weight are mainly used as the main parameters of the proportioning test. The actual rock formation parameters and similar model parameters are listed in Table 2.

Similar model material selection principle

For the five main materials of quartz sandstone, shale, iron ore body, diorite, and backfill involved in the stratigraphic range, the final similar model material is river sand as aggregate, gypsum, and calcium carbonate are used as cementing materials, and barite powder is used as weight gain material, plus water. Among them, the gypsum is made of ordinary gypsum
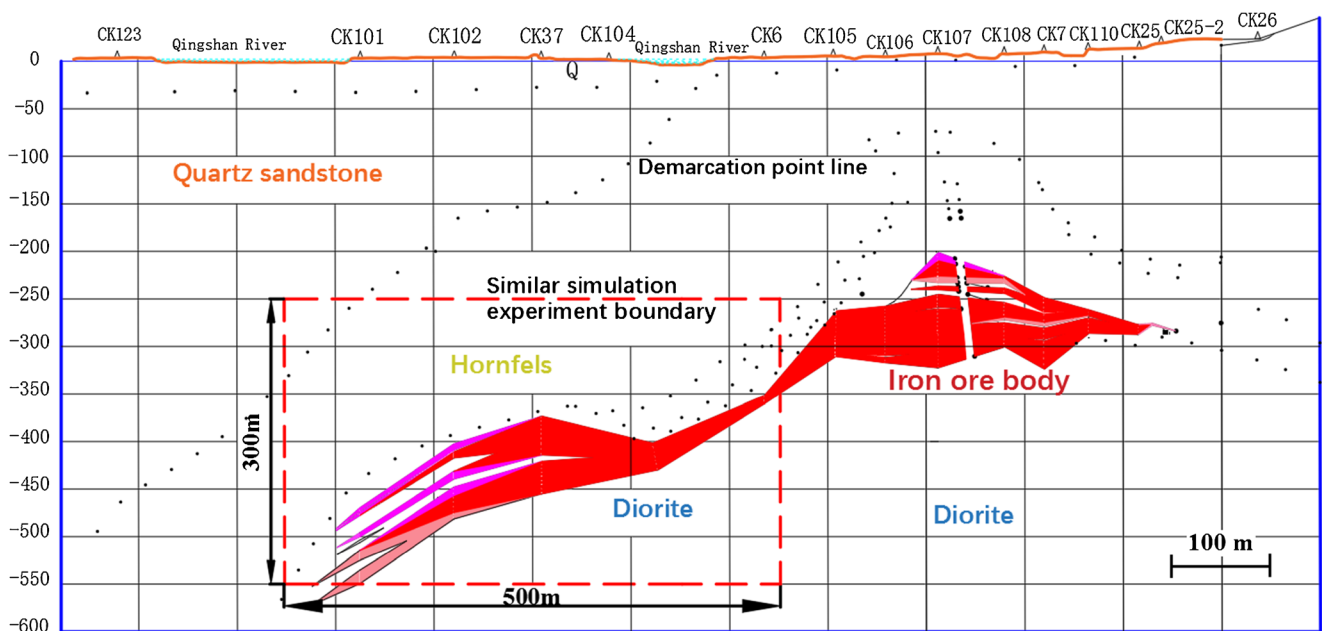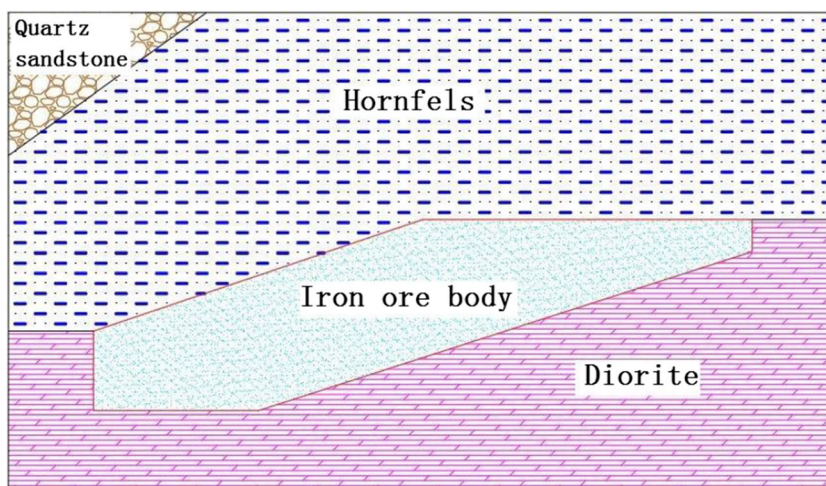

Fig. 1 Geological profile of No. 1 exploration hole in Baixiangshan Iron Mine

Fig. 2 Similar model diagram

powder, which has the characteristics of quick solidification. Calcium carbonate is selected from 400~600 mesh heavy calcium carbonate. The material is a cementitious material with a certain viscosity, and the strength is usually below 1.0 MPa. The weight-increasing material is selected from the fineness of 400~600 mesh barite powder, and the barite powder is also called barium sulfate powder, and the density is generally $\geq$ 4.0g/cm^3. The aggregate is made of fine river sand. The river sand should be dried before the test to avoid the ratio error. In order to make the material as homogeneous as possible, the river sand sieve is divided into fine river sand with a particle size of less than 1 mm before use. Calcium carbonate and gypsum are moisture-proof before use.

Similar model material ratio test

A total of 75 standard test pieces were prepared, with a specification of φ50 mm × 100 mm, as shown in Fig. 3. After the test piece was produced, it was cured for 7 days at an average room temperature of 18 °C. After that, the uniaxial compressive strength test was performed using a CMT5305 microcomputer controlled electronic universal testing machine.

The barite powder not only plays a decisive role in the volume-weight of the material, but also has a certain influence on the strength of the barite powder. With the decrease of the sand-glue ratio, the uniaxial compressive strength of the material decreased overall. In every five groups of materials with a fixed sand ratio, the uniaxial compressive strength of the material increases significantly as the gypsum powder accounts for the specific gravity of the cemented material. After the material was added with water, the viscosity was enhanced and the difficulty of mixing was gradually increased. Therefore, the material containing the barite powder should be thoroughly mixed and the tensile strength affected by it should be taken into consideration to avoid experimental errors.

First, the test results in Table 3 were compared and analyzed with the mechanical parameters (uniaxial compressive strength and volume-weight) of similar materials in the actual rock formation in Table 2. Then, the proportion numbers 873+ 10%, 964+10%, 673+40%, and 873+10% were selected to simulate quartz sandstone, angle shale, iron ore body, and diorite respectively. River sand was used as an aggregate similar to the filling body, and a certain proportion of calcium

Table 1 List of completed workload of field survey

Work projects		Unit	Quantity
Drilling		m	1213.00
Pumping test		hole	2
Sonic test		Point	480
Ground temperature test		m	670
Water quality analysis		Piece	2
Rock physical and mechanical properties test	Block density test	Piece	122
	Uniaxial compressive strength test	Group	60
	Direct shear test	Group	60
	Brazil split	Group	60
	Sonic wave speed test		60

Table 2 Mechanical parameters of model materials

Rock formation type	Actual parameter						Model parameter	
	Density (kg/m^3)	Elastic modulus (GPa)	Uniaxial compressive strength (MPa)	Cohesion (MPa)	Internal friction angle (°)	Poisson's ratio	Density (kg/m^3)	Uniaxial compressive strength (MPa)
Quartz sandstone	2910	17.43	35.40	3.2	38.1	0.19	1940	0.118
Hornfels	3002	13.34	27.90	2.72	32.3	0.26	2001	0.093
Iron ore body	3999	23.70	36.60	4.13	51.4	0.16	2466	0.132
Diorite	2880	29.84	34.80	3.32	57.4	0.21	1920	0.116
Gray sand ratio 1:8 cemented backfill	1830	6.00	1.00	0.35	20	0.42	1220	0.003

carbonate and retarder were added to make it have a certain shape to meet its low strength (uniaxial compressive strength: 0.003MPa) and easy to fill the goaf.

Displacement and stress monitoring methods

Displacement measurement method

Digital Photo Deformation Measurement Technology (DPDM) is an advanced practical measurement technology that uses high-resolution digital cameras as data acquisition tools to realize deformation measurement and analysis on computers using image analysis methods (Li et al. 2006).

The strain high-precision digital camera deformation measurement technology adopted by China University of Mining and Technology consists of an ordinary digital camera, a light source system, and a software analysis system. The software system consists of an image analysis program PhotoInfor and a post-processing program PostViewer, as shown in Fig. 4.

Fig. 3 Specimens of similar materials

Table 3   Test results for similar material specimens

Group	Matching number	Density (kg/m^3)	Uniaxial compressive strength (MPa)	Group	Matching number	Density (kg/m^3)	Uniaxial compressive strength (MPa)
1	637+0%	1850	0.253	14	864+0%	1815	0.079
2	646+10%	2013	0.136	15	873+10%	1973	0.118
3	655+20%	2122	0.210	16	937+30%	2244	0.217
4	664+30%	2231	0.343	17	946+40%	2438	0.201
5	673+40%	2449	0.134	18	955+0%	1826	0.077
6	737+10%	1973	0.154	19	964+10%	2011	0.099
7	746+20%	2265	0.172	20	973+20%	2116	0.077
8	755+30%	2329	0.132	21	1037+40%	2487	0.184
9	764+40%	2482	0.139	22	1046+0%	1962	0.066
10	773+0%	1863	0.065	23	1055+10%	2103	0.082
11	837+20%	2085	0.242	24	1064+20%	2210	0.133
12	846+30%	2266	0.234	25	1073+30%	2323	0.108
13	855+40%	2438	0.195				

Notation: For example, the ratio of 764+40% indicates that the material has a sand-binder ratio of 7:1, the calcium carbonate content is 60% of the total amount of cemented material, and the gypsum content is 40% of the total amount of cemented material; the barite powder content is 40% by weight of the aggregate

The deformation monitoring and analysis of this experiment was completed using the equipment system.

The high-resolution images of each mining stage were collected by a digital camera according to a certain time series or a series of mining stages. The collected numerical images were analyzed by related analysis software to obtain displacement images of surrounding rock. Therefore, in a similar experiment, the surface displacement of the surrounding rock in the mining area can be obtained after real-time photographing with a digital camera.

Stress measurement

In order to monitor the variation of the stress between the surrounding rock and the middle section of the ore body, a total of 30 standard pressure cells were used to dynamically monitor the vertical stress of each mining stage. The pressure cell was arranged at intervals of 25 cm in the horizontal direction, and 10 pressure cells were arranged for the upper and lower plates, respectively, and the pressure cell was placed at a vertical distance of 5 cm from the top and bottom of the ore body. Five pressure
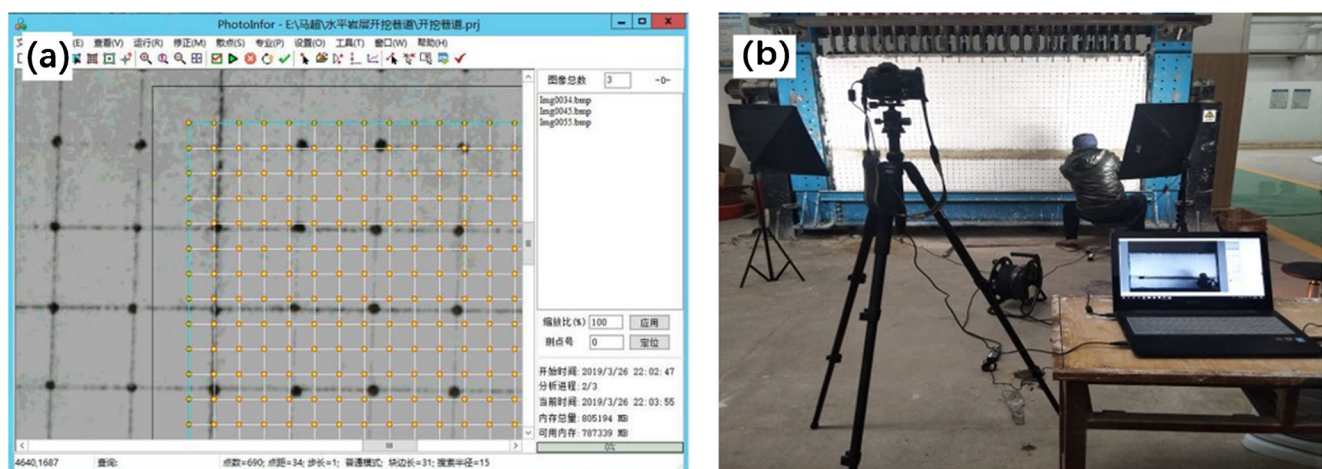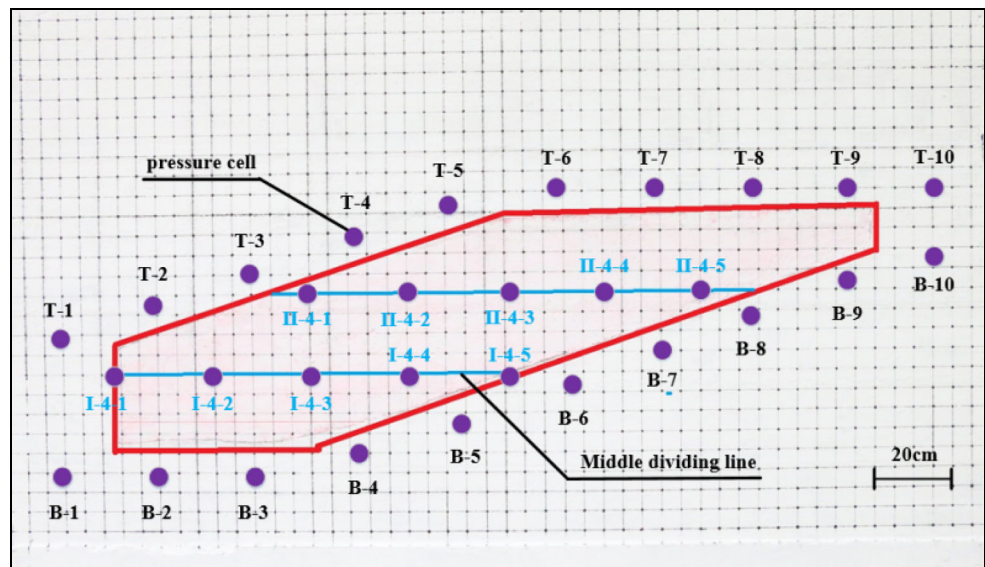

Fig. 4 Digital photography-based deformation measurement system. Notation: **a** Image Analysis System PhotoInfor. **b** Camera system

Fig. 5 Location design of pressure cell embedding

cells were arranged in each middle section of the stope. The pressure cell layout is shown in Fig. 5. The data acquisition adopts the static strain test analysis system with the specification of TST3826F-L. The acquisition system is shown in Fig. 6.

External compensation pressure

The actual mining model range of the mine is −250m∼−550m, which corresponds to a similar model height of 1.5 m. Therefore, according to the similar material simulation conditions, the model load tester top loading system was used to provide the static load required for external force compensation to achieve the stress under similar buried depth conditions. The vertical stress that should be applied in this model is:

$$\sigma_v = \gamma H C_F = 0.025 MPa \tag{5}$$

where γ is the average volume-weight of the overburden, and the value is 30.00 kN/m³; H is the buried depth, and the value is 250 m; C_F is the stress similarity ratio.

Mining plan

MMSCBM was adopted as a mining plan for similar model tests. This physical model was divided into three middle sections according to the actual mining level of the Baixiangshan Iron Mine. The upward layered approach cemented filling mining method was adopted in the middle section. The middle section has a height of 40 m and a stratified height of 10 m. Each middle section was divided into 4 layers, and the filling stage length of each layer mining was set to 50 m. The middle section was mined from deep to shallow, and the first middle section leads the next middle section of the first layer of mining, and the layers were immediately filled at the end of mining. According to the actual mining sequence of the mine, the

Fig. 6 Static strain test and analysis system

mining sequence will be transitioned from a single mid-segment to a multi-segment mining. The specific sequence was divided into six mining stages, after the first stage: mining I-1 layer; after the second stage: mining I-2, II-1 layer; after the third stage: mining I-3, II-2, III-1 layer; after the fourth stage: mining I-4, II-3, III-2 layers; after the fifth stage: mining II-4, III-3 layers; after the sixth stage: mining III-4 layers. The middle layer of the ore body is shown in Fig. 7.

Analysis of surrounding rock disturbance failure process

The morphological evolution process of the overburden structure during the excavation process was photographed by the camera. At the same time, after completing the filling of each mining stage, the disturbance of the surrounding rock was drawn into a sketch in order to clearly observe the failure of the surrounding rock structure, as shown in Fig. 8a.

As shown in Fig. 8a, due to the small mining distance, the filling body effectively limited the settlement deformation and failure of the overburden. The mining only caused the small area to fall and the tiny cracks at the top plate position, and the surrounding rock disturbance was small.

In the early stage of the second-stage mining, a separation crack occurred at the ore-rock interface of the hanging wall, and a horizontal crack appeared in front of the roof of the mining approach, as shown in Fig. 9a. After the second-

Fig. 8 Disturbance and failure map of surrounding rock in multi-middle ▶ mining. Notation: **a** Model state and scene sketch after the first stage; **b** Model state and scene sketch after the second stage; **c** Model state and scene sketch after the third stage; **d** Model state and scene sketch after the fourth stage; **e** Model state and scene sketch after the fifth stage; **f** Model state and scene sketch after the sixth stage; DF is delamination fracture, CZ is collapsed zone, FEA is falling empty area, LEA is layered empty area, and FIEA is filling empty area

stage mining, the ore body above the layer II-1 produced obvious separation cracks along the interface between the upper ore body and the surrounding rock and develops upward, as shown in Fig. 8b. The angle of the crack was gradually reduced, and finally developed into a horizontal separation crack away from the goaf filling area. Due to the uneven sinking of the overburden, vertical cracks were created at the rightmost end of the horizontal delamination crack. Due to the support of the filling body, the vertical crack stopped growing at a certain distance above the goaf filling area, and finally the crack in the layer was "trapezoidal" arched. The integrity of the horizontal pillars was better. Only a small number of tiny cracks that developed upwards from the vertical top plate were generated at the upper layered roof and the lower layered bottom plate and were not penetrated. Prior to this, the stope was in the stable phase of the pillar.

As shown in Fig. 8c. After the completion of the third stage mining, the horizontal pillar between the middle section I and the middle section II had obvious bending and sinking, similar
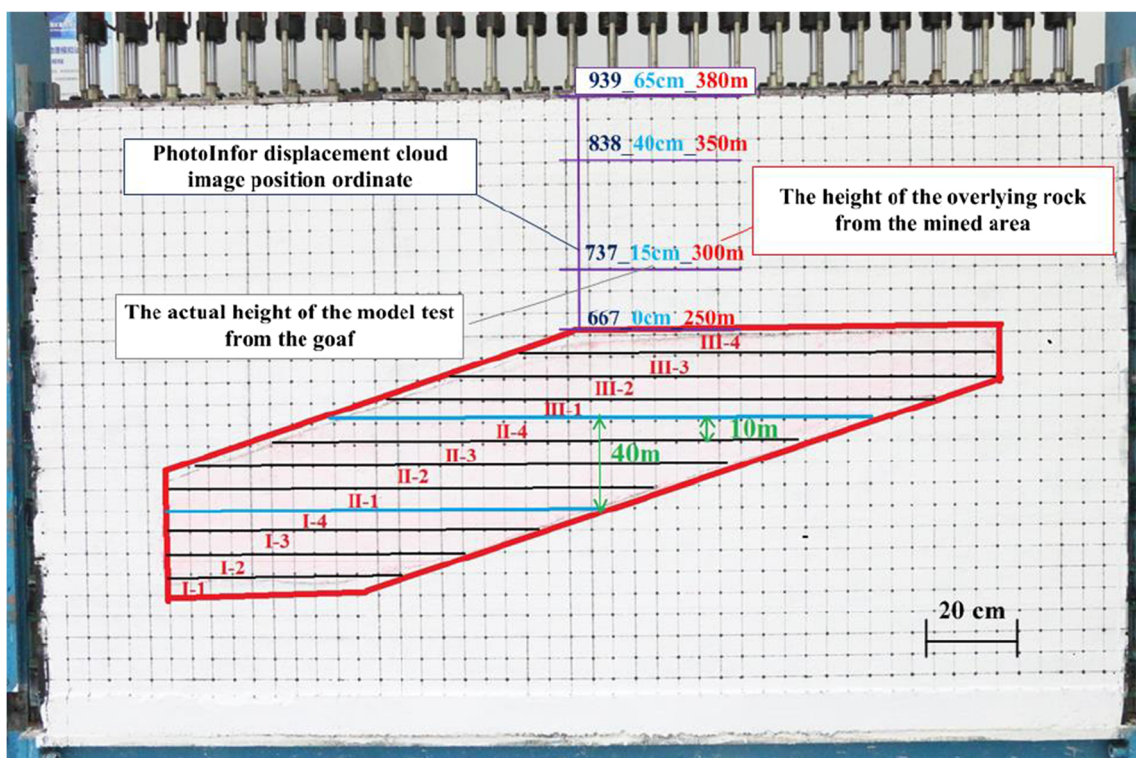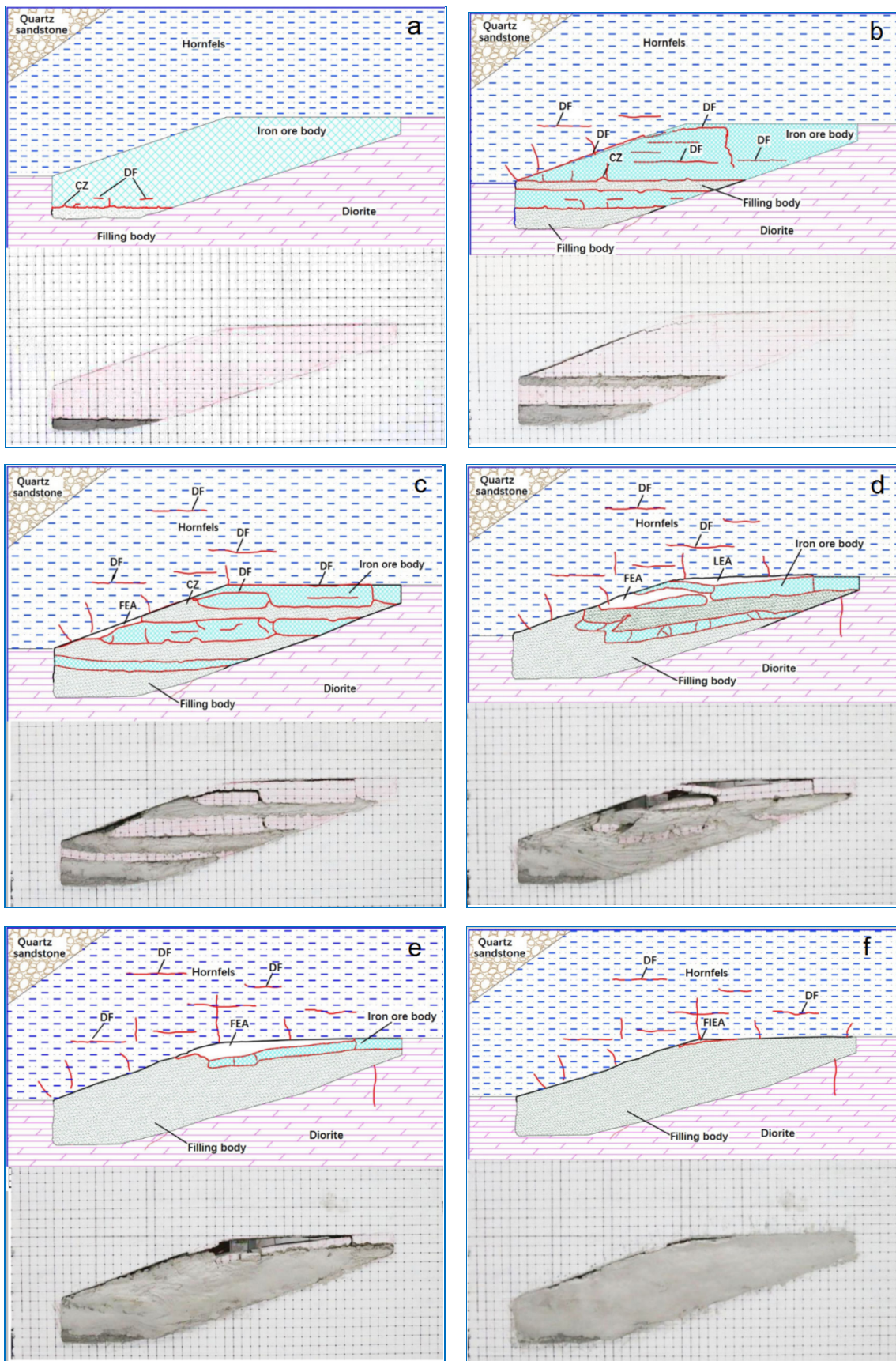

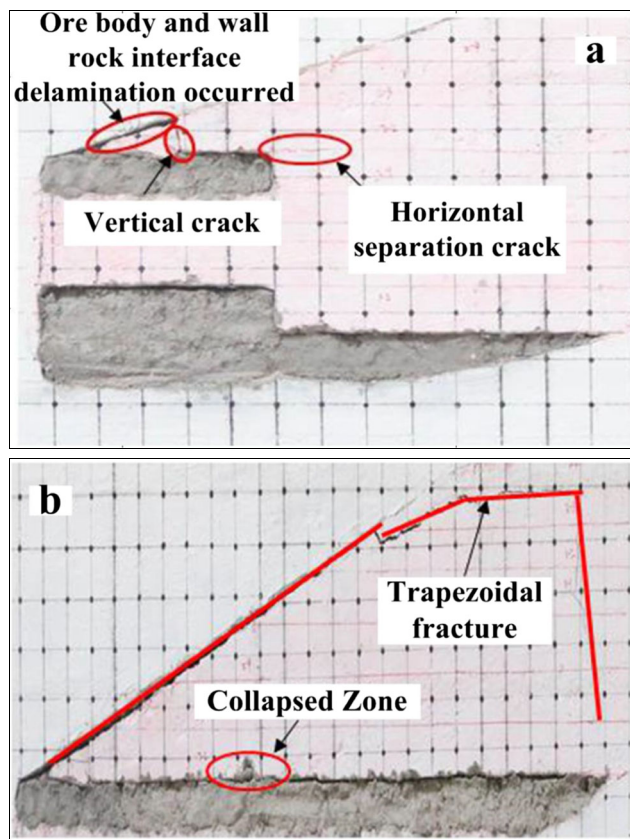**Fig. 7** Schematic map of mid-level stratification of ore body

Fig. 9 Overburden movement deformation and failure map

to the statically indeterminate beam fixed at both ends and subjected to load deformation, so it can be called "rock beam." Due to the bending and sinking of the "rock beam," the middle section II stope body was subjected to the overall sinking deformation, and its own compression deformation, eventually causing the filling to not be topped. The integrity of the pillar between the middle section II-2 and III-1 was obviously deteriorated, and the interface between the ore body and the surrounding rock produces a fracture crack that was obviously penetrating up and down, which was in the middle of the pillar. According to Figure 9b, the development of local fissures in the third stage can be found more clearly, and the most obvious is the further development of "trapezoidal" arched fissures. The settlement deformation of the overlying strata on the left side of the stope was always larger than that on the right side, which leaded to the further increase of the width and length of the separation crack at the interface between the overlying strata and the ore body above the middle section III. This separation crack extended to the right side of the section of the ore body, causing the goaf filling area to penetrate with the ore body. The interbedded fissures on the overburden increased and the vertical fissures began to sprout. At this time, the stope is in the stage of large deformation of the pillar.

As shown in Fig. 8d, since the horizontal pillars between the middle section II and the middle section III do not have

bearing capacity, the uneven subsidence deformation of the horizontal pillars caused the integrity of the original filling body above the pillars to be destroyed. As the filling body deformed with the sinking of the pillar, it also produced separation and caving. The original separation crack on the left side of the III-2 layer ore body was further increased, resulting in a larger area of falling empty area and layered empty area. The vertical fracture of the overburden was further increased. At this time, the stope was in the stage of partial pillar failure.

As shown in Fig. 8e, after the end of the fifth stage mining, the three middle-stage goaf filling areas were connected to each other, and the remaining layered ore bodies had obvious fractures. The variation of the separation crack and vertical fracture on the overburden was not obvious. At this point, the stope was in the stage of failure of the overall pillar. As shown in Fig. 8f, the sixth stage mining is the III-4 layer. There is no significant change in the number, width, and length of horizontal cracks in the overburden due to settlement deformation. Due to the large area of mining and filling, the filling body was obviously separated from the overlying rock layer after a long time of self-compression deformation, and the filling empty area was generated in a small area.

The above analysis of the four stages of MMSCBM: the stage of the stable pillars, the stage of the large deformation pillars, the stage of partial pillars failure, and the stage of failure of the overall pillars. During the mining process, a temporary horizontal pillar was formed between the upper and lower sections, which carried and isolated the filling body, and had a lateral restraining effect on the overlying rock. At this time, it played a major role in maintaining the stability of the stope; Furthermore, the thickness of the temporary horizontal pillar was getting smaller and smaller until the self-stability was lost, and the load on the filling body was getting larger and larger. The filling body acted as a temporary horizontal pillar that slowed down the temporary horizontal pillar destruction speed and eventually carried the damage. The filling body and the temporary horizontal pillar were arranged in isolation, and the surrounding rock was combined to form a frame supporting structure. This structure effectively slowed down and weakened the deformation and failure of the surrounding rock and overburden, and is of great significance for maintaining the overall stability of the stope.

Analysis of stress disturbance law

As shown in Fig. 10, the vertical position of the pressure plate on the upper plate is 5 cm from the top plate of the similar model ore body. Therefore, the vertical stress value of each test point of the overburden at a vertical distance of 10 m from the roof of the stope can be obtained by using the conversion monitoring data, as shown in Fig. 5. The vertical stress change curves of the surrounding rocks of the upper and lower walls of each mining stage were drawn, with the number of the
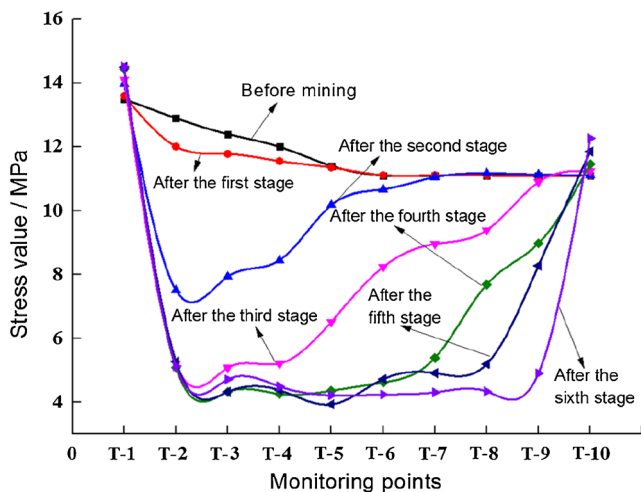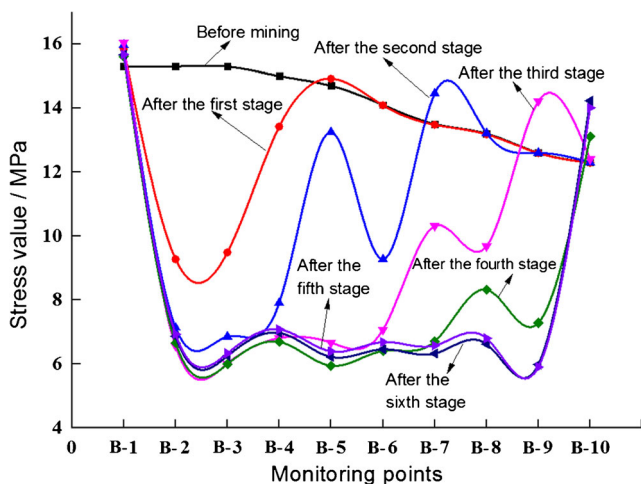
Fig. 10 The vertical stress of the surrounding rock on the hanging wall varies with the mining stage

As shown in Fig. 11, as the mining and filling progresses, the vertical compressive stress of the surrounding rock of the lower plate gradually decreased, forming a "W"-shaped stress relief zone. During the primary three stages of mining, the stress release of the surrounding rock was large and the whole fluctuates, and the impact was less in the later stage of mining. The stress concentration on both sides of the surrounding rock was obvious. The stress values are 15.67 MPa and 14.22 MPa, respectively, and the stress growth amplitudes are 0.34 MPa and 1.66 MPa, respectively.

The position of the pressure cell between the middle sections is the intermediate position of the I-4 layer and the II-4 layer, and the vertical distance from the layered upper and lower interface is 2.5 cm, which is converted to the actual intermediate distance of the project is 5.0 m, as shown in Fig. 7.

As shown in Fig. 12 and Fig. 13, the temporary horizontal pillar formed by multi-middle mining has a positive effect on controlling the deformation of the goaf. During the process of thinning and horizontal disappearance of the horizontal pillars, the horizontal pillar stress was gradually released smoothly, the stress distribution was uniform, and the overall sudden instability of the horizontal pillars does not occur.

monitoring point as the abscissa, as shown in Fig. 10 and Fig. 11.

As shown in Fig. 10, with the mining and filling of each mining stage, the vertical stress value of the overlying rock in the goaf gradually decreased, forming a "U"-shaped stress relief zone. The span of the "U"-shaped stress relief zone gradually expanded to the right as each mining stage progresses, and its expansion speed and stress reduction amplitude were greatly affected by different mining stages. The maximum stress reduction amplitudes from the first stage to the sixth stage were 0.89 MPa, 4.50 MPa, 3.60 MPa, 3.61 MPa, 2.49 MPa, and 3.37 MPa, respectively. As the mining stage progresses, the vertical stress on both sides of the upper wall of the goaf filling area increased, resulting in stress concentration. After the end of mining, the vertical stress of $1^{\#}$ measuring point and $10^{\#}$ measuring point increased by 1.00 MPa and 1.15 MPa respectively before mining.

Displacement law of overlying strata

Through the PhotoInfor image processing software independently developed by China University of Mining and Technology, the overburden displacement tracking analysis was carried out, so that the dynamic process of the overburden sinking movement in the simulated mining stage was completely revealed by the displacement cloud map, as shown in Fig. 14. The specific position of the ordinate in Fig. 14 is the position marked by the dark blue value in Fig. 7. The position
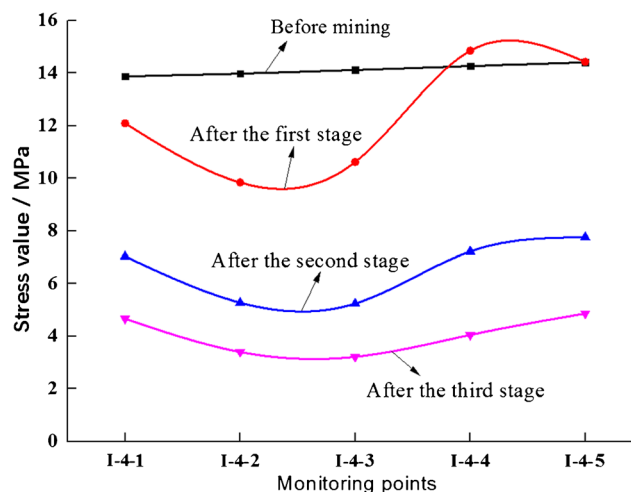

Fig. 11 The vertical stress of surrounding rock in the footwall varies with the mining stage

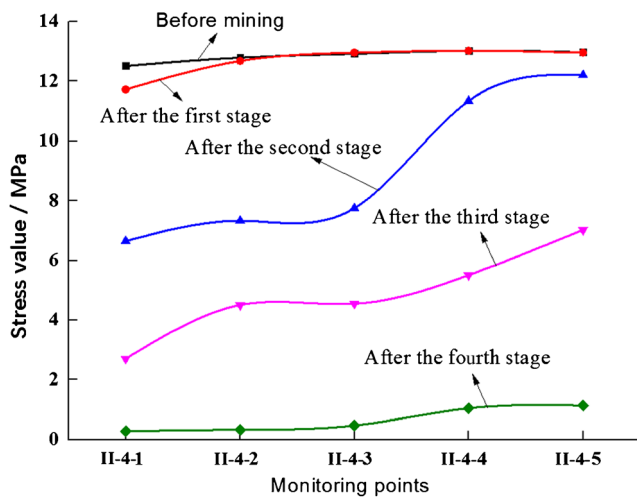**Fig. 12** Vertical stress change diagram of **I**-4 layer

Fig. 13 Vertical stress change diagram of **II**-4 layer

marked by the light blue value in Figure 7 represents the height of the overburden of the similar model. The position marked by the red value in Figure 7 represents the height of the overlying rock in the actual project.

As shown in Fig. 14, with the progress of each mining stage, the maximum vertical displacement of overburden was always located directly above the goaf, and then gradually expands to both ends and the upper part as the mining progresses. Four lines are taken from the lower 0-cm, 15-cm, 40-cm, and 65-cm heights of the image processing range, and the actual conversion to the prototype is buried depth −380 m, −350 m, −300 m, and −250 m, as shown in Fig. 7. According to the displacement data monitored by PhotoInfor image processing software, the curve of displacement variation of overlying strata in each mining stage was plotted, as shown in Fig. 15.

As can be seen from Fig. 15, the variation of the vertical displacement of the overburden during MMSCBM process is as follows: (1) The vertical displacement of each rock layer increases gradually with the mining stage, and the displacement of the direct top rock stratum is the largest in the goaf; (2) The vertical displacement of the direct top of the goaf varies greatly, and there is a sudden change. This is because the direct top rock layer is disturbed by excavation, so that the goaf is close to the air surface and the rock layer is fractured or

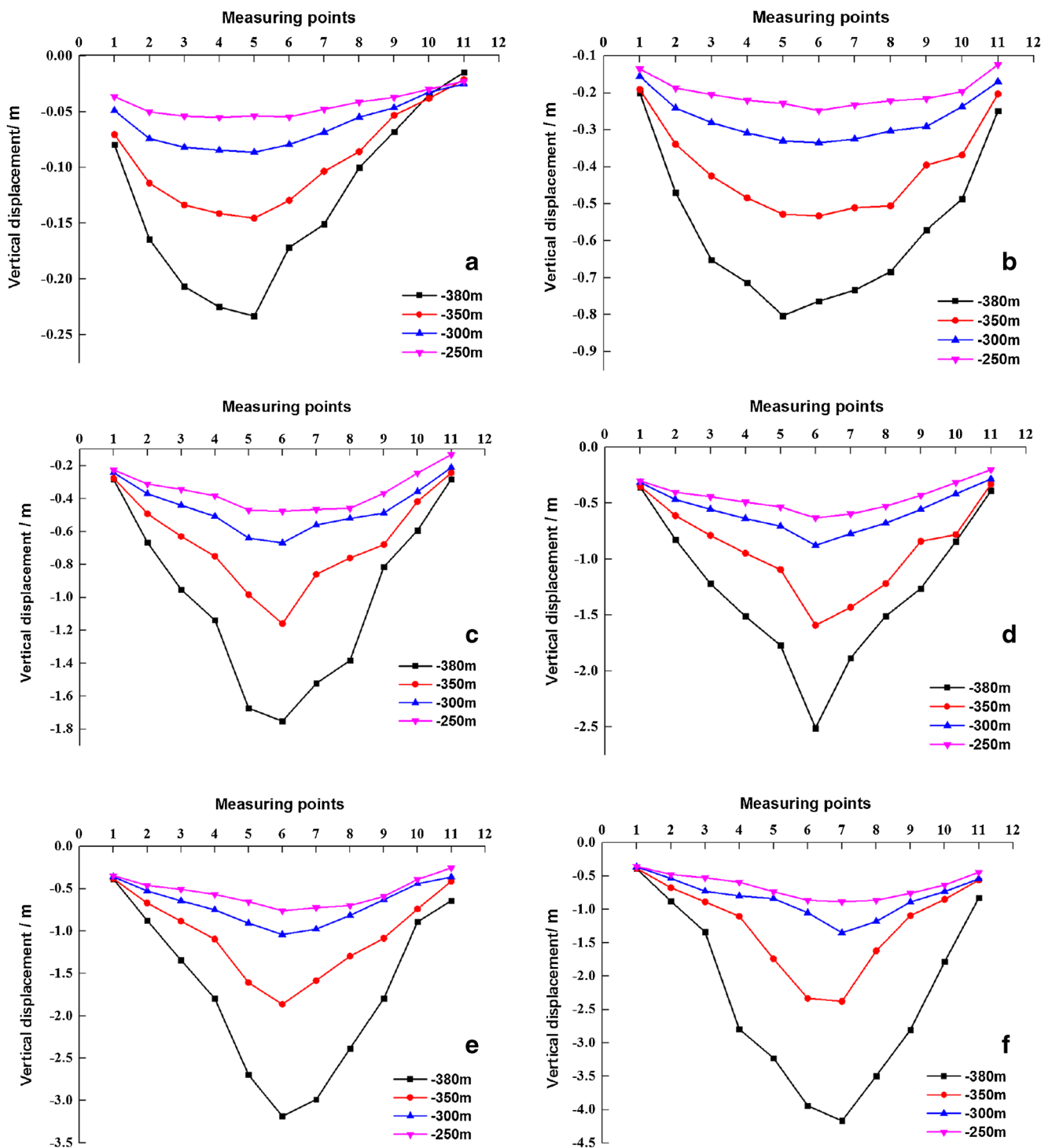Fig. 14 Vertical displacement cloud map of overburden rock in each mining stage
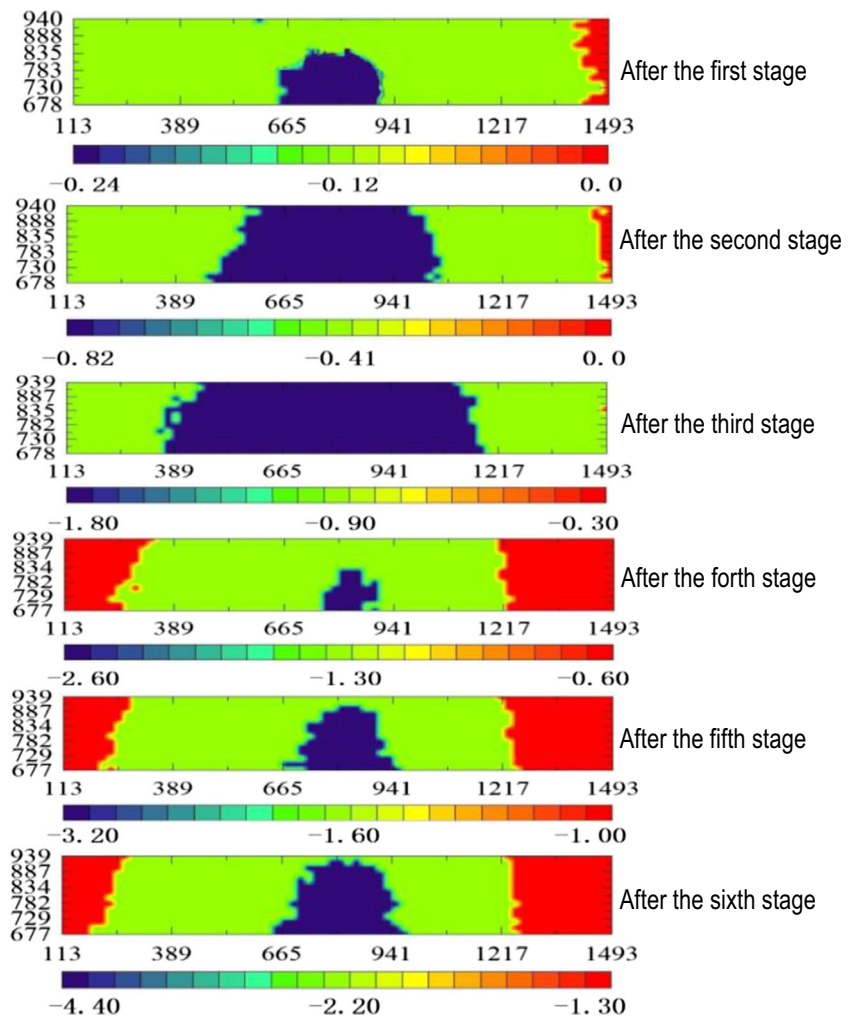
Fig. 15 Vertical displacement curve of overburden in each mining stage. Notation: **a** After the first stage; **b** After the second stage; **c** After the third stage; **d** After the fourth stage; **e** After the fifth stage; **f** After the sixth stage

even collapsed, and the rock layer has discontinuous displacement changes. (3) The asymmetry of overburden subsidence is obvious. The closer to the goaf, the more obvious the asymmetry of rock subsidence. (4) The maximum vertical displacement of each mining stage is located in the upper middle part of the goaf, and gradually moves to the right with the mining stage, and decreases along the rock surface facing the left and right boundaries. (5) The vertical displacement of the overlying strata decreases with the distance from the goaf, and the development of the fissures is less obvious.

The maximum vertical displacement of different rock layers in each mining stage was fitted, as shown in Fig. 16.
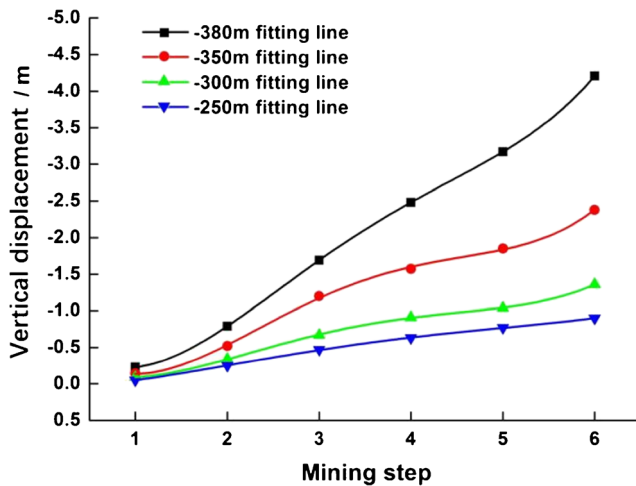
Fig. 16 Maximum vertical displacement curve of overburden rock in each mining stage

The maximum vertical displacement of each rock layer gradually increases with the progress of the mining stage. The closer to the goaf, the greater the vertical displacement of the rock formation and the faster the rate of growth. The growth rate of vertical displacement of the same rock layer increases first, then decreases, and then increases, and the closer to the goaf, the more obvious the trend.

Numerical simulation study

Calculation model establishment

The calculation model was established mainly based on the No. 1 main ore body in the western positive contact zone between the exploration holes of CK101~CK105 in Baixiangshan Iron Mine. The length of the strike of the model (z direction) is 860m, and the tendency (x direction) is taken according to the actual size of the ore body in the simulation range. The width of the model is about 6 times the width of the ore body. The vertical direction of the model is the y axis. The three-dimensional calculation model has a size of 1300 m
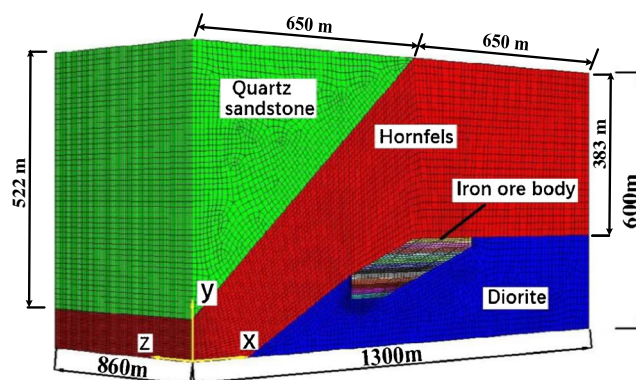

Fig. 17 Numerical model

(length) × 860 m (width) × 600 m (height), and a total of 579, 124 cells and 600, 126 nodes were divided. The model was built as shown in Fig. 17. The model adopted the displacement boundary condition, and the top is the surface free boundary and the overburden self-weight was applied. According to the ground stress measurement of the mine site, the side stress coefficient is taken as 0.8, and the Mohr-Coulomb yield criterion is used for calculation. The contact surface under the condition of giving smaller cohesion parameters was set at the boundary between the ore body and the surrounding rock mass. The mechanical parameters used in the model calculation are shown in Table 2.

Analysis of simulation results

Based on the simulation calculation of MMSCBM process, the three-dimensional analysis of the surface settlement of each mining stage was obtained, as shown in Fig. 18.

As shown in Fig. 18, the maximum settlement of the surface gradually increases with the mining stage, by analyzing the three-dimensional settlement map. The settlement amount is along the direction of the ore body, and the tendency is a gentle "hat" shape with a small intermediate end. With the mining, the center of the maximum settlement value gradually expands to the right along the tendency, and finally, after the end of the sixth stage mining, a maximum settlement area which is biased to the right is formed directly above the ore body. When the mining reaches the third stage or the fourth stage, the surface settlement reaches a high level, and gradually stabilizes when the mining is after the fifth stage or the sixth stage. This law is consistent with the vertical displacement of similar simulated overburden. The maximum settlement amount from the first stage to the sixth stage is as follows: −0.02 m, −0.13 m, −0.26 m, −0.33 m, −0.37 m, −0.38 m, the tendency of increase is first increased and then decreased, and the overall change is gentle and sedimentation. The amount is small, and the impact on the ground is small, as shown in Fig. 19. The relative deformation rate of the overlying surface is $0.365/380 = 0.096\% < 0.1\%$, and the safety is good (Li et al. 2013; Lu and Gao 2003; Jiang et al. 2018).

Analysis of variation law of overburden displacement

The rock monitoring lines from 0 to −380 m from the top were set up to reveal the influence of MMSCBM on the movement of the overlying rock, as shown in Fig. 20.

The dynamic settlement curve of the rock formation has been calculated, as shown in Fig. 21.

As shown in Fig. 21, with the shortened distance to the goaf, the apparent vertical displacement curve of the overburden shows obvious asymmetry. The main reason for the
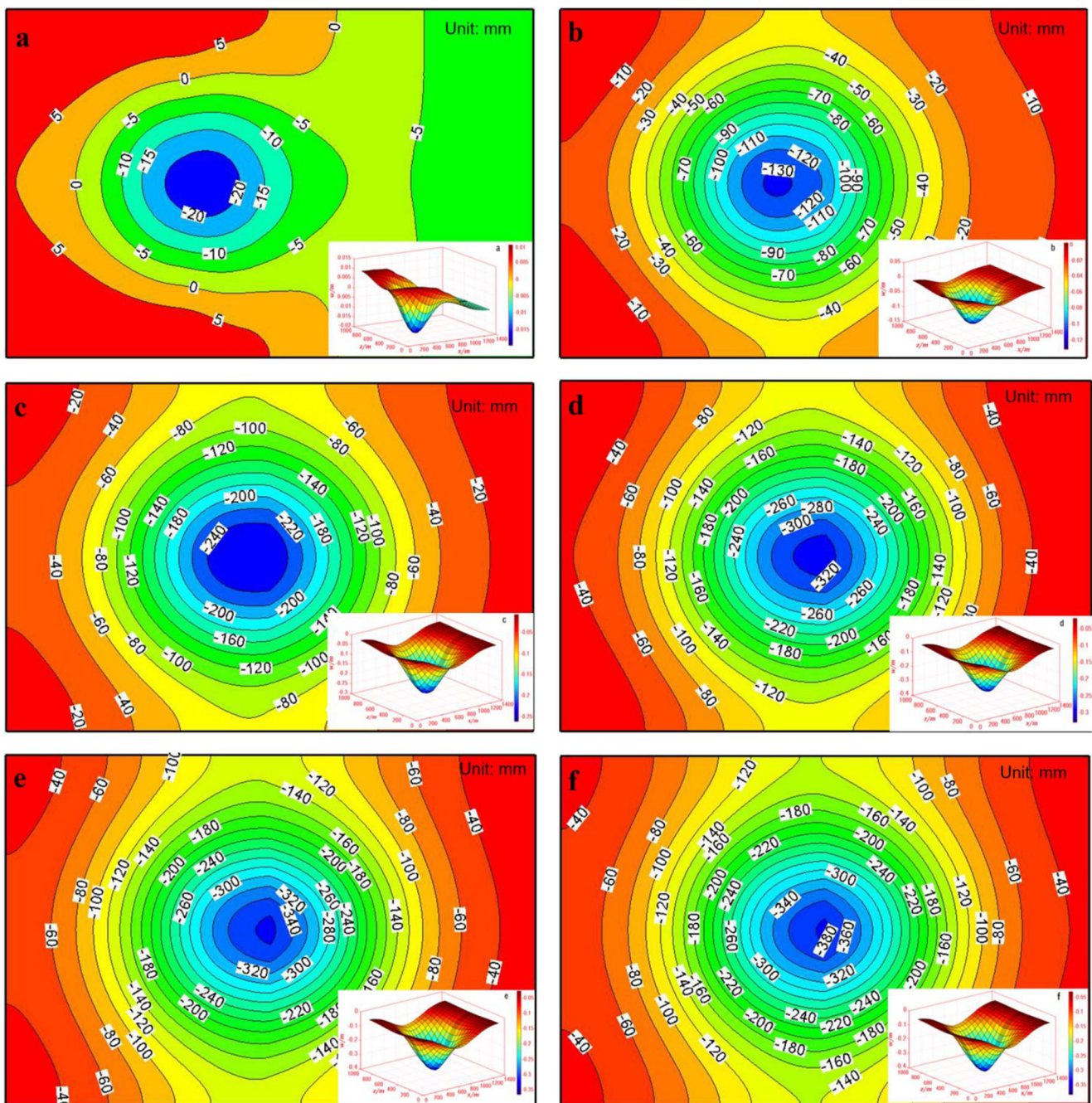
Fig. 18 Three-dimensional map of settlement in each mining stage. Notation: **a** After the first stage; **b** After the second stage; **c** After the third stage; **d** After the fourth stage; **e** After the fifth stage; **f** After the sixth stage

asymmetry is that the closer the distance to the goaf is, the worser the integrity of the overburden is, as a result of the asymmetry of the fracture of the roof stratumand and the discontinuous displacement of the stratum and local abrupt changes. In continuous mining operations, the macroscopic performance of the movement, deformation, and failure of the overlying strata always lags behind the excavation itself. This is mainly because MMSCBM effectively buffers the intensity of the interference impact caused by mining, and its purpose is to divide continuous mining into partial mining. In

the early stage of mining, unmined ore bodies are mainly affected by mining interference. In the later stage of mining, mining disturbances are mainly buffered by filling bodies. As a result, the progress of movement and deformation of the overlying rock layer is reduced and slowed down.

Figure 22 shows the relationship between the maximum vertical displacement of the rock mass and the distance h from the rock formation to the roof of the stope. The distance from the rock formation to the top of the stope is a variable, and the maximum vertical
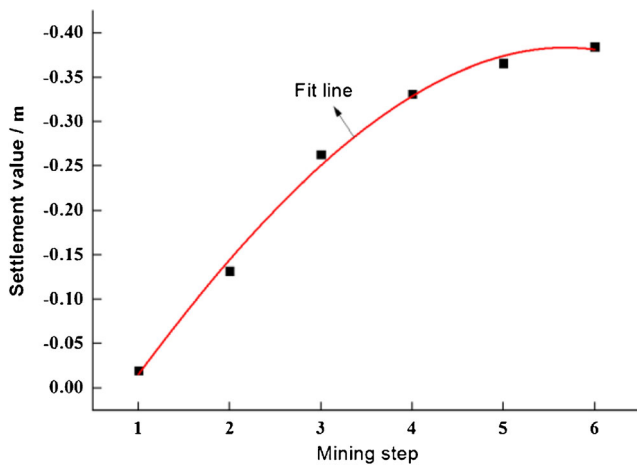
Fig. 19 Maximum settlement of the surface with the mining stage

Fig. 21 Vertical displacement curve of overlying rock at different depths under each mining stage

displacement w of the rock formation is fitted by the following formal formula:

$$w = a \times e^{-x/b} + c \tag{6}$$

where a, b, and c are fitting parameters. The resulting fitting results are shown in Eq. 7.

$$w = -0.0017 \times e^{-h/49.74} - 0.449$$

$$R^2 = 0.997 (\text{correlation coefficient}) \tag{7}$$

From the fitting results, we can see that: the maximum vertical displacement of the rock mass varies exponentially with the distance from the rock to the roof. The vertical displacement of the overburden decreases with the increase of the distance h from the roof. The vertical displacement of the overburden is the largest at the top plate position, which is

−3.940 m, and the smallest at the surface, which is −0.384 m, and the vertical displacement difference between the two adjacent rock layers is also gradually reduced. The disturbance effect caused by mining is gradually weakened as the overlying strata propagate to the surface. The increase of overburden thickness and depth of mining has the effect of reducing surface subsidence.

Comparison of numerical simulation and similar test results

After the end of the mining, the vertical displacement curves of the rock layers at different depths obtained by numerical simulation and similar model test monitoring were compared and analyzed, as shown in Figures 23 and 24.
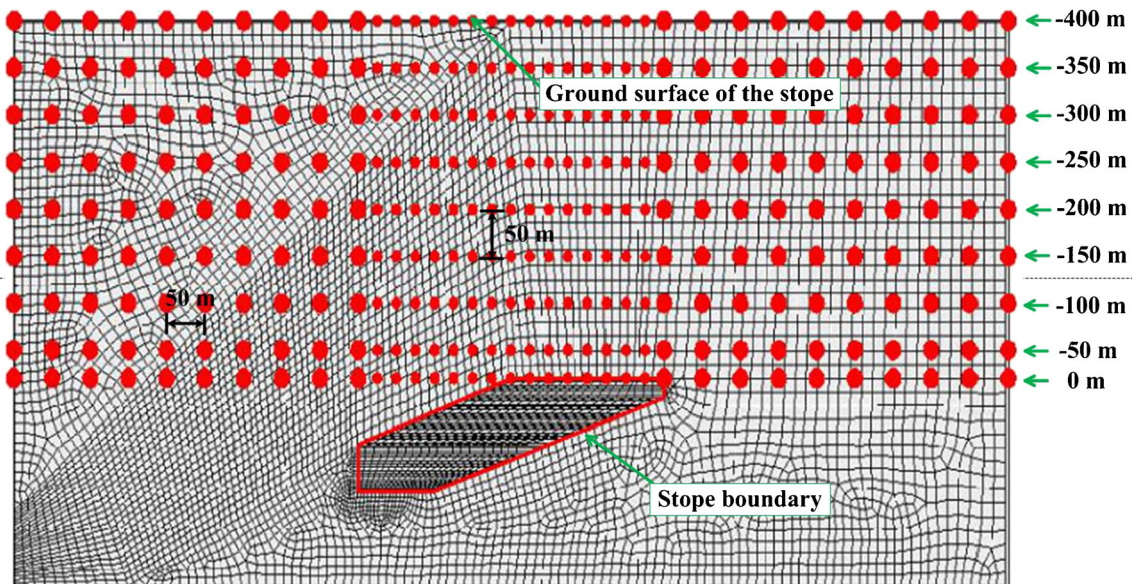

Fig. 20 Distribution of monitoring points in numerical simulation of overlying strata
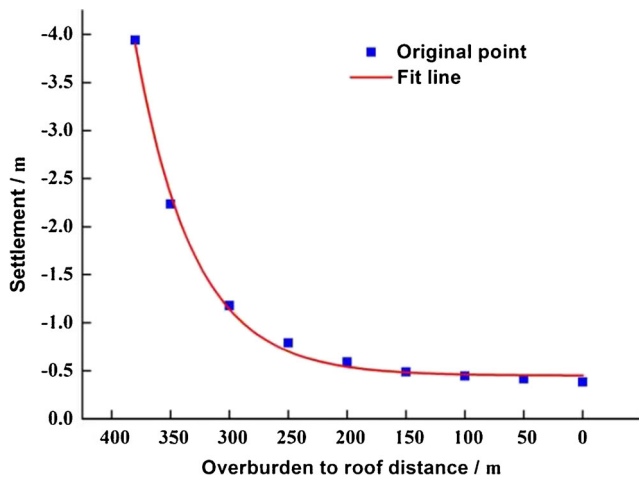
Fig. 22 Maximum settlement of different buried depths of overlying rock

Fig. 24 Vertical displacement of overlying rock at different depths of numerical simulation monitoring

From the overall perspective, the similar simulation monitoring results are basically consistent with the numerical simulation monitoring results. The number of similar test monitoring points is much less than that of the numerical simulation monitoring points. The monitoring length is the maximum range of the ore body, and the numerical simulation monitoring length is within the range of 3 times the maximum range of the ore body, which results in the overall variation of the numerical simulation results. The monitoring results are gentle, but the actual vertical displacement is the same. The vertical displacements of the rock formations at the depths of −250 m, −300 m, −350 m, and −380 m obtained by numerical calculation and similar simulation monitoring are −3.92 m, −2.24 m, −1.18 m, and −0.79 m, respectively. The vertical displacements of the rock formations at −250-m, −300-m, −350-m, and −380-m depths were −4.17 m, −2.38 m, −1.35 m, and −0.89 m, respectively. From the vertical displacement of rock strata at different depths, the numerical calculations are basically consistent with the results of similar model
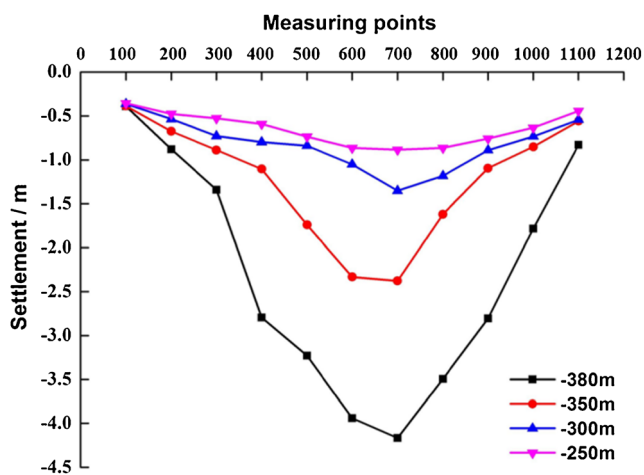

Fig. 23 Vertical displacement of overlying rock at different depths monitored by similar tests
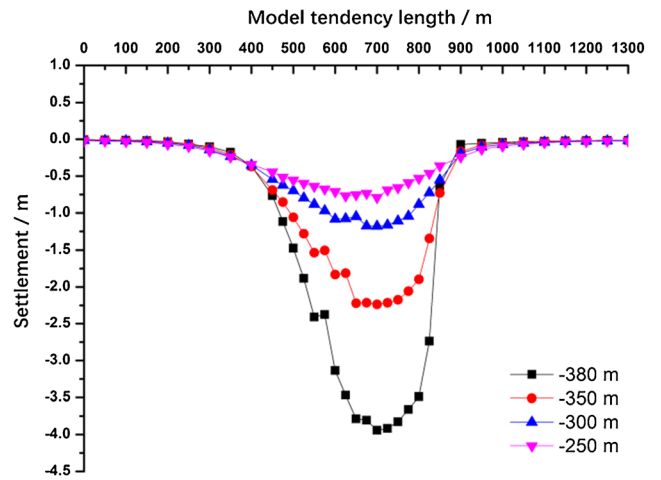
tests. The two methods can verify each other in the study of MMSCBM.

After the ore body was mined, the plastic failure of the surrounding rock mainly occurred in the roof and floor of the goaf and the surrounding rock at the left and right sides, as can be seen from Figure 25. In the initial three mining stages, plastic failure of surrounding rock mainly occurred in the upper ore body, left and right roof and floor surrounding rocks, and horizontal ore pillars in the goaf. The shape of the ore body plastic failure zone in the upper part of the goaf was arched, that is, a balanced pressure arch structure was formed in the roof rock. The balanced pressure arch structure can effectively bear the weight of the overlying strata and control the propagation of mining influence to the surface. The pressure arch of the roof of the goaf developed from bottom to top, followed by tensile failure area, shear failure area, and undamaged area. Among them, the tensile failure area was the largest, and the closer to the goaf, the easier it is to break and collapse. The surrounding rocks of the left and right roof and floor of the goaf were mainly sheared. Horizontal pillars were mainly tensile failure and had a large thickness at the initial stage of formation. From the middle to the two ends, the horizontal pillars developed into tensile failure areas, shear failure areas, and undamaged areas in sequence. The distribution of plastic failure areas made the pillars show an "X"-shaped failure trend, as shown in Fig. 27c.

In the last three mining stages, plastic failure of surrounding rock mainly occurred in the surrounding rock of the roof of the goaf. As mining progresses, the area of the plastic damage zone gradually increased. The filling body fills the goaf in time, reducing the exposed area of the roof, so the roof surrounding rock was mainly sheared. The impact of underground mining will eventually spread to the surface, causing the surface to move and deform. From the evolution of the plastic zone of the model at each mining stage, it was found that during first stage mining, the surface plastic zone was
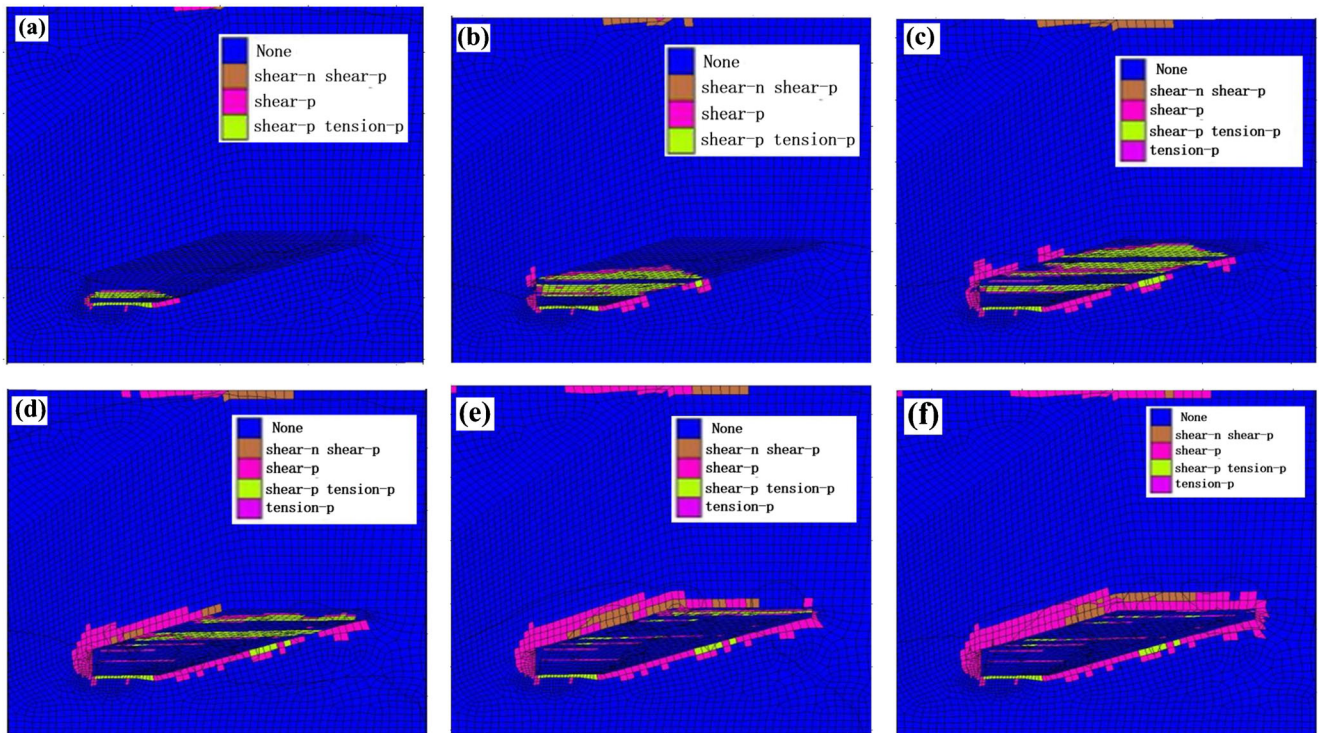
Fig. 25 Development map of surrounding rock plastic zone in each mining stage. Notation: **a** After the first stage; **b** After the second stage; **c** After the third stage; **d** After the fourth stage; **e** After the fifth stage; **f** After the sixth stage
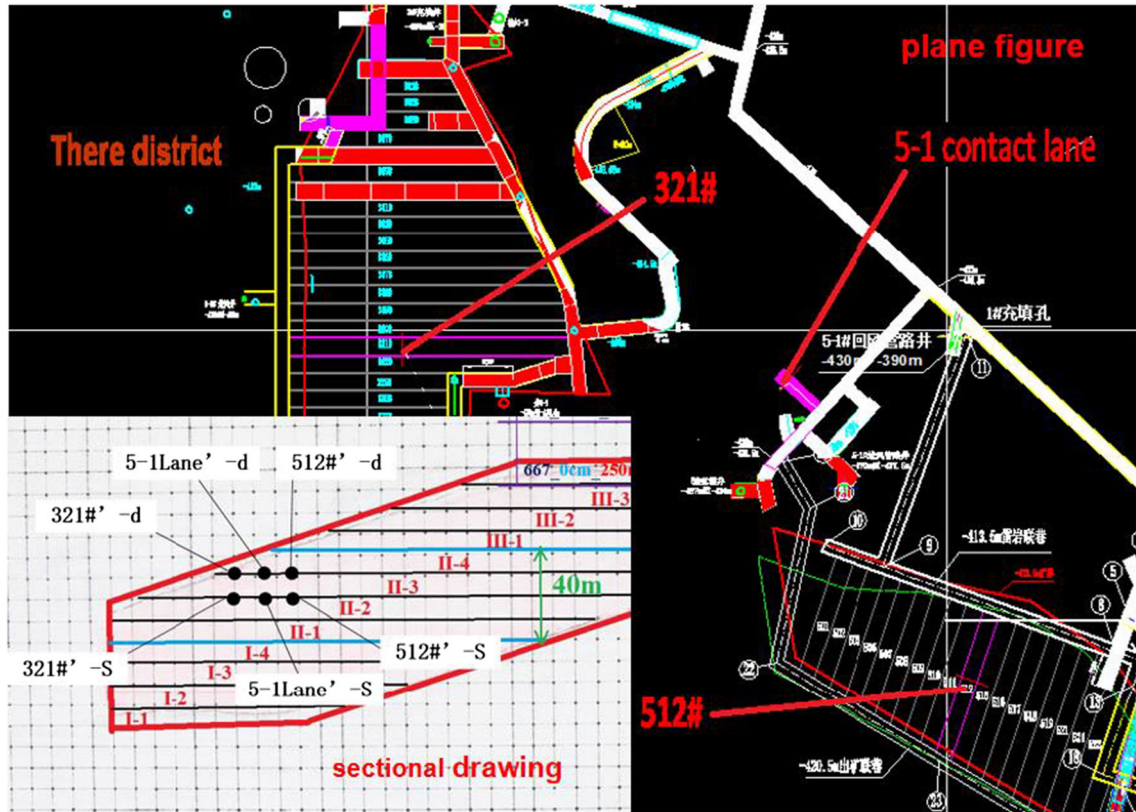

Fig. 26 Location of the roadway monitoring section

Fig. 27 Arrangement of measuring points in the roadway monitoring section. Notation: **a** Schematic diagram of the arrangement of convergence deformation points; **b** Arrangement of convergence deformation points on-site; **c** Schematic diagram of the separation of the top layer separation points; **d** Arrangement of measuring points of the roof on-site
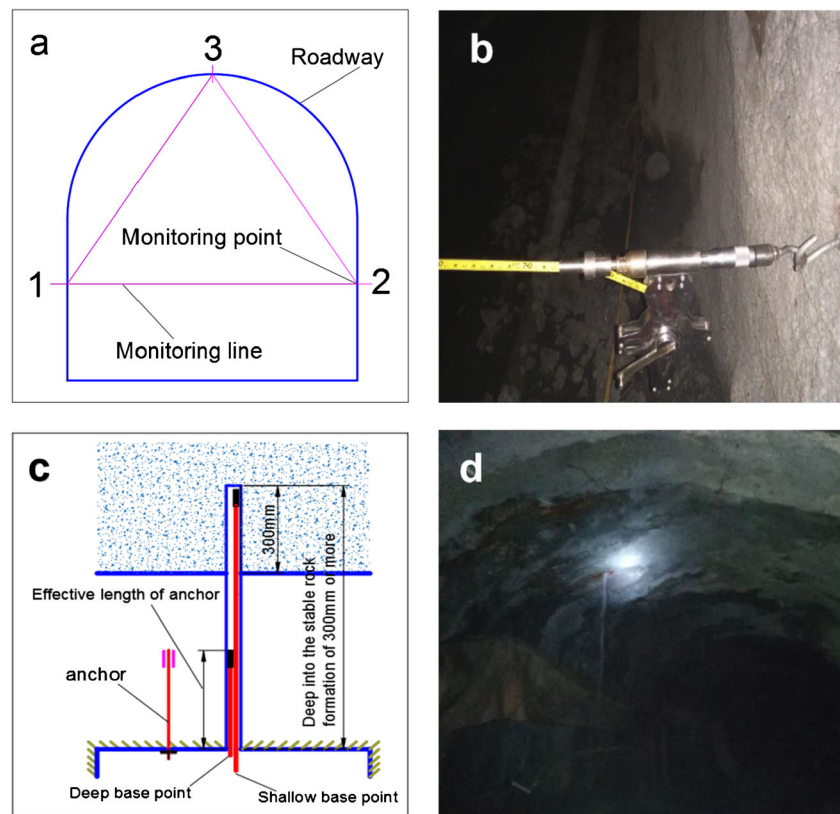
located directly above and to the right of the inclination center of the ore body. As the mining progresses, the plastic zone gradually extended to both ends and the scope gradually increased. Finally, after the sixth stage mining was over, the distance between the two ends of the surface plastic zone extending from the center of the orebody's inclination is almost equal. In each mining stage, the surface was mainly sheared, as shown in Fig. 25d~f.

The results of numerical calculations are basically consistent with the characteristics of surrounding rock movement and failure in similar model experiments, which were analyzed from the perspective of the development process of plastic zone failure in surrounding rock, as shown in Fig. 8. The difference is that the failure characteristic of this rock mass in the similar model test is a discontinuous abrupt development, while in the numerical calculation it is a continuous gradual development.

Field deformation observation

Local roadways were monitored for the convergence and deformation of surrounding rock and roof separation. The dynamic deformation of surrounding rock and its regularity were analyzed in order to guide mine road construction and predict danger. Numerical simulation calculations were carried out to verify the correctness of on-site monitoring. −440 level

(between the II-2 and II-3 layer) 321[#] mine room access road, 512[#] mine room access road, and 5-1 lanes were selected for monitoring of surrounding rock convergence and deformation and roof separation monitoring. The on-site monitoring period is the period from the start of the second stage mining in the similar model test to the completion of the third stage mining. Figure 26 shows the location of the roadway plan where the monitoring point is located and the model section where the numerical simulation monitoring point is located. The arrangement of measuring points in the monitoring section is shown in Figure 27.

The on-site monitoring results show that the cumulative deformation of the horizontal displacement of 512[#] Mining Road, 321[#] Mining Road, and 5-1 Lane Road reaches 12.85 mm, 8.62 mm, and 4.78 mm respectively; The cumulative amount of vertical displacement of the roof of 512[#] Mining Road, 321[#] Mining Road, and 5-1 Lane Road reached 6.53 mm, 5.58 mm, and 3.06 mm, respectively, as shown in Figure 28. From the numerical simulation monitoring results, it can be seen that the cumulative amount of vertical displacement of the roof of 512[#'] Mining Road, 321[#'] Mining Road, and 5-1 Lane' Road reached 6.796 mm, 6.046 mm, and 5.77 mm, respectively, as shown in Figure 29.

As shown in Figure 30, the on-site monitoring separation values of the deep base points of 512[#] Mining Road, 321[#] Mining Road, and 5-1 Lane are 3.68 mm, 3.10 mm, and 2.41 mm respectively. The on-site monitoring separation

Fig. 28 Convergence deformation monitoring of surrounding rock of roadway section
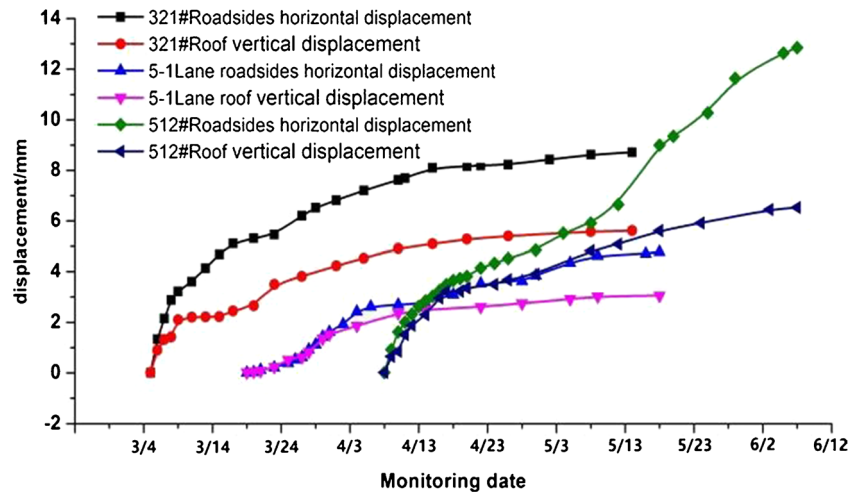
values of the shallow base points of 512# Mining Road, 321# Mining Road, and 5-1 Lane are 2.26 mm, 1.55 mm, and 1.62 mm respectively. Relatively speaking, the numerical simulation results of the deep base points of 512#' Mining Road, 321#' Mining Road, and 5-1 Lane' Road are respectively 4.40 mm, 3.71 mm, and 1.87 mm, as shown in Figure 31.

The above shows that the difference between on-site monitoring and numerical simulation calculation is relatively small in terms of the results of the vertical displacement of the roof and the value of roof separation. This shows that on-site monitoring has considerable accuracy. The difference is that numerical simulation can realize monitoring from the first stage of excavation, while on-site monitoring can only be monitored after excavation. Therefore, different roadways of on-site monitoring data have a certain sequence over time. According to the analysis of the monitoring results, the impact on surrounding rock in the early stage of excavation is slightly stronger than in the later stage, and gradually weakened and stabilized in the later stage. The displacement and deformation

of the surrounding rock are all small, which indicates that the excavation disturbance is less affected. Existing mining filling schemes and supporting schemes can effectively control the surrounding rock deformation of the mining access (mining house).

The former Soviet scholars obtained the approximation formula for calculating the maximum allowable vertical displacement value of the ceiling of the cavern through the compilation of a large number of observation data:

$$\delta_1 = 12 \times \frac{b_0}{f} \tag{8}$$

where f is the Platts coefficient, $f = R/10$, R is the uniaxial compressive strength of the rock, and the uniaxial compressive strength of the ore is 36.6 MPa; b_0 is the span of the cavity, taking a minimum of 4.7 m. The calculated value of δ_1 is 15.41 mm and the maximum vertical displacement of the top plate is 6.53 mm. The relative safety factor is 2.36, so the roadway stability is very high.
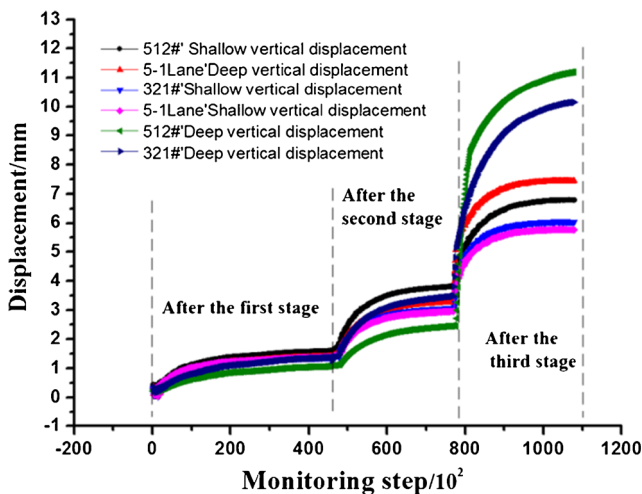
Conclusion

1. When performing MMSCBM, the process of surrounding rock disturbance and failure can be divided into the stage of the stable pillars (after the second stage), the stage of the large deformation pillars (after the third stage), the stage of partial pillars failure (after the fourth stage), and the stage of failure of the overall pillar (after the fifth stage). The mining mode relies on the structure of the temporary horizontal pillar and the filling body to slow down and weaken the deformation and damage of the surrounding rock, the pillar, and the overlying strata, and helps to maintain the overall stability of the stope.

2. With the mining and filling of each mining stage, the vertical compressive stress value of the overburden in

Fig. 29 Numerical simulation results of the vertical displacement of the roof

Fig. 30 Delamination monitoring of the roof of the roadway
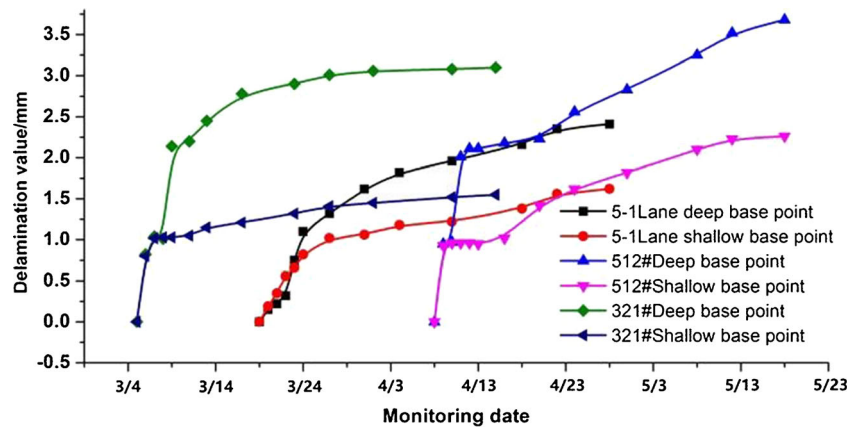
the goaf gradually decreased, forming a "*U*"-shaped stress release zone, and the maximum decreasing amplitude first increased and then stabilized; The vertical compressive stress of the surrounding rock forms a "*W*"-shaped stress relief zone, and the maximum decreasing amplitude increased first and then decreased. The vertical stress of the temporary horizontal pillar of the stope had been gradually released smoothly, avoiding the sudden break. The stress concentration area was initially distributed in the middle pillar and finally transferred to the four corners of the goaf filling area. The transfer of the stress concentration area effectively shortens the stress accumulation time in the stress concentration area to extend the safe mining time of the mining area.

3. The numerical results and similar experiments were compared in the vertical displacement of the overburden and the surrounding rock disturbance, and the correctness of the two methods is verified. The research on the surface settlement and the horizontal displacement of the surface shows that MMSCBM has less surface disturbance and the surface safety meets the normative standard.

4. The on-site monitoring results have been verified by numerical simulation calculations, indicating that they have considerable accuracy. Based on the analysis of on-site monitoring results and numerical simulation results, the displacement of the mining area and the roadway is small, and the relative safety factor is 2.36. The disturbance of the roadway by MMSCBM can be maintained by supporting means and can maintain high safety.

Declarations

Conflict of interest The authors declare that they have no competing interests.

References

Copland T, Nehring M (2016) Integrated optimization of stope boundary selection and scheduling for sublevel stoping operations. J S Afr Inst Mining Metallurgysn 116:1135–1142

Deng YY, Chen CX, Xia KZ, Yang KY, Sun CY, Zheng XW (2018) Investigation on the characteristics of overlying strata caving in the Chengchao Iron Mine, China. Environ Earth Sci 77(10):362

Emad MZ (2017) Numerical modelling approach for mine backfill. Sadhana 42(9):1–10

Emad MZ, Mitri H, Kelly C (2015) State-of-the-art review of backfill practices for sublevel stoping system. Int J Surf Min Reclam Environ 29(6):13

Feng F, Li DY, Li XB, Guo ZP, Wang SF, Chen Y (2017) Novel underhand cut-and-fill stoping method and mechanical analysis of overlying backfill. Int J Geomech 17(7):1–15

Jiang FF, Zhou HL, Sheng J, Shuai JS, Sun DS, Hu Y, Li XD (2018) Analysis and evaluation of surface deformation characteristics under
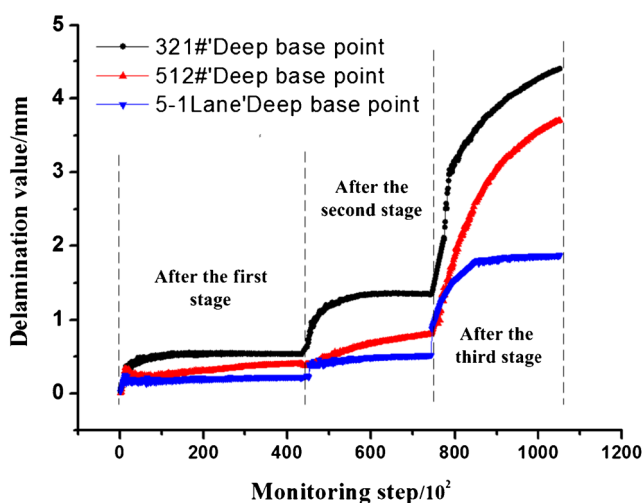
Fig. 31 Numerical simulation results of roof separation

the condition of completely backfill mining. Chin J Rock Mech Eng 37(10):2344–2358 [in Chinese]

Kurakami T, Yamatomi J, Sato R, Sagawa Y, Murakami S (2008) Mining with backfill at the Hishikari Mine, Japan. Gospod Surowcami Min 24:197–212

Lan SZ, Hou YB, Fan PF (2015) Numerical analysis on the failure mode of stage backfill stope due to mining disturbance. Adv Mater Res 1089:239–243

Li YH, Jing HW, Zeng QY (2006) Development and application of digital photogrammetry software package for geotechnical engineering. Yanshilixue Yu Gongcheng Xueba. Chin J Rock Mech Eng 25(2):3859–3866

Li XB, Li DY, Liu ZX, Zhao GY, Wang WH (2013) Determination of the minimum thickness of crown pillar for safe exploitation of a subsea gold mine based on numerical modelling. Int J Rock Mech Min Sci 57(1):42–56

Li LC, Tang CA, Zhao XD, Cai M (2014) Block caving-induced strata movement and associated surface subsidence: a numerical study based on a demonstration model. Bull Eng Geol Environ 73(4): 1165–1182

Lu QS, Gao Q (2003) Monitoring research on convergence deformation of laneway way rock and obsturator in no.2 digging of Jinchuan. Chin J Rock Mech Eng 22(SUPPL.2):2633–2638 [in Chinese]

Song WD, Wang DX, Tang YN (2011) Study on sublevel open stoping with subsequent backfilling mining method stope parameters optimization. Adv Mater Res 250-253:1567–1571

Uskov VA, Kondrat'ev SA, Neverov SA (2017) Economic expediency of copper ore mining with waste rock fill of secondary stopes in the west wing of the Oktyabrsky deposit. J Min Sci 53(6):1090–1095

Xu WB, Song WD, Tan YY, Wang YD, Wang WJ (2012) Failure mechanism of stope and exploited areas with stage backfill method in metal mine. J China Coal Soc 37(SUPPL.1):53–58(6) [in Chinese]

Xu S, Suorineni FT, An L, Li Y (2017) A study of gravity flow principles of sublevel caving method in dipping narrow veins. Granul Matter 19(4):82

Yang YK, Ma YR, Ji CX, Kang TH, Guo XY (2018) Effect of mining thickness on overburden movement and underground pressure characterics for extrathick coal seam by sublevel caving with high bottom cutting height. Adv Civil Eng 32:1–15

Yi CP, Sjöberg J, Johansson D (2017) Numerical modelling for blast-induced fragmentation in sublevel caving mines. Tunn Undergr Space Technol 68:167–173

Yu TR, Counter DB (1983) Backfifill practice and technology at Kidd Creek Mines. Can Min Metall Bull 76:56–65

Zhang XF, Tao GQ, Zhu ZH (2018) Laboratory study of the influence of dip and ore width on gravity flow during longitudinal sublevel caving. Int J Rock Mech Min Sci 103:179–185

Zhu W, Xu J, Xu J, Chen D, Shi J (2017) Pier-column backfill mining technology for controlling surface subsidence. Int J Rock Mech Min Sci 96:58–65